Conductance of nanotube junctions and its scaling law

Ryo Tamura and Masaru Tsukada
Department of Physics, Graduate School of Science, University of Tokyo, Hongo 7-3-1, Bunkyo-ku, Tokyo 113, Japan
(Received 26 March 1996; revised manuscript received 5 November 1996)

The conductance of junctions connecting two different metallic carbon nanotubes is calculated by Landauer's formula with a simple tight-binding model. The structures of the junctions are characterized by the relative positions of a pair of disclinations, i.e., a five-membered ring and a seven-membered ring. Conductances of about six thousand kinds of junctions are obtained. The conductance is determined only by the ratio R_2/R_1 where R_1 is the the circumference of the thinner tube and R_2 is that of the thicker tube. When $R_2/R_1 \gg 1$, the conductance is found to be almost proportional to $(R_2/R_1)^{-3}$. The wave function in the junction also shows a power-law decrease as a function of the distance measured from the thinner tube. [S0163-1829(97)03108-1]

I. INTRODUCTION

Recently, one-dimensional structures called carbon nanotubes have been discovered and have attracted much interest.[1] Structures related to the nanotubes have been also found, which include helically coiled nanotubes,[2,3] junctions between nanotubes,[4] and cap structures.[5] Disclinations are key ingredients to generate the curved graphitic sheet forming these three-dimensional nanostructures. Here the disclinations mean n-membered ring ($n \neq 6$) defects in the otherwise hexagonal lattice of two-dimensional (2D) graphite. It forms a center of positive (negative) curvature when $n<6$ ($n>6$), and causes a variety of structures made by graphite sheets such as fullerenes,[6] minimal surfaces structures,[7]and torus structures.[8] The disclination is a sort of topological defect: their distribution on the honeycomb lattice causes the change of the topology in the bond network of carbon atoms. Compared to the problems of local potential disorders, the effects of the topological disorder on the electronic state and the quantum transport have not been well investigated so far, in particular, for the honeycomb lattice.

Among these structures, the nanotube junction is important as a part of more complex structures, e.g., double junctions and multiple junctions, which are candidates of electronic devices with nanometer size. In the double junction where a semiconductor tube is connected between two metallic tubes, the semiconductor tube will behave as a bottle neck part, through which electrons are transmitted only by tunneling. A sequence of such weak junctions might work as a single electron tunneling transistor of the nanometer scale.[9] The single junction itself also might behave as a weak junction in certain cases, and scattering properties at the joint should afford an important base for the study of general more complex junctions. Though we have already obtained local density of states around a disclination in the monolayer graphite,[10] they are not enough for the discussion about transport phenomena through the nanotube junctions. Therefore we attempt in the present paper to develop a theoretical method for the transport properties of electrons through nanocages of graphitic sheet and apply it to the single junction formed by two metallic nanotubes.

Recently, some theoretical calculations about the nanotube junctions have been reported.[11,12] Saito and co-workers calculated the conductance of the nanotube junctions, but they use finite cluster models for the calculation.[11] Such a boundary condition is not suitable for calculating the conductances, when the mean free path of the electron is longer than the cluster size. In this case, the nanotubes in both sides of the junctions should be treated as semi-infinite ones. Because, otherwise, general properties of ballistic electron transport cannot be discussed. Chino and co-workers treated semi-infinite nanotubes in the junctions, but they treat only fused pentagon-heptagon pairs.[12] Both authors of Ref. 11 and Ref. 12 have treated only several junctions. Therefore, any systematic dependence of the ballistic transport on the junction size and shape has not been clarified enough. In the present paper, in contrast to it, the conductances of about six thousand junctions are systematically calculated. These include a number of different structures with widely ranging values of length of junctions, various combinations of helicities, and diameters of the tube parts. The most remarkable result of the present paper is a scaling rule which generally holds in all the cases. It can be simply expressed that the conductance is determined only by the ratio of R_2/R_1, where R_2 and R_1 are the circumference of the thicker tube and that of thinner tube, respectively. Furthermore, the conductance σ is expressed in the form of $(R_2/R_1)^{-3}$ for the larger values of R_2/R_1.

The outline of the paper is as follows. In the next section (Sec. II) the models of the junction and the method for calculation of the conductance are described. In Sec. III, the result of the calculated conductances are presented and the observed scaling law is analyzed with a simple phenomenological arguments.

II. METHOD FOR CALCULATION

Figure 1 shows bars representing zig-zag segments of the C-C bond network in the circumferential direction of the single junction. They are aligned and numbered along the direction $\vec{e}_1 - \vec{e}_2$, where $\vec{e}_1$ and $\vec{e}_2$ are the unit vectors of the graphite plane. Each bar is connected with adjacent bars by the remaining C-C bonds. The network is rolled up so that the atoms in the top and the bottom of the same bar become the identical one. The top atoms and the bottom atoms are represented by filled circles and open circles in Fig. 1(b),

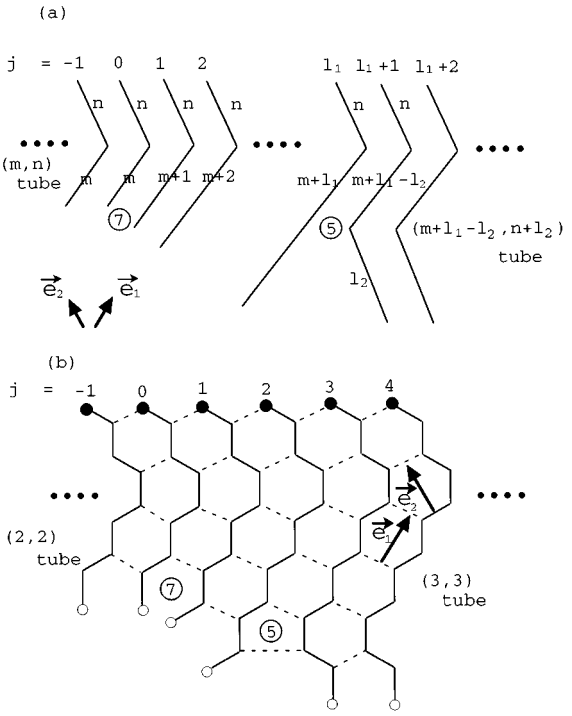

FIG. 1. (a) The development map showing the bond networks of the (m,n)-$(m+l_1-l_2,n+l_2)$ junction. It is represented by aligned bars. Figures 5 and 7 in circles show the positions of the five-membered ring and seven-membered ring, respectively. (b) The development map showing the bond network of the (2,2)-(3,3) junction. The filled circle at the top and the open circle at the bottom in each bar indicate an identical atom. To form the junction, the development map is rolled up so that the filled circle and the open circle coincide with each other in each bar.

respectively. The structure of the bar j for $j\leqslant 0$ is formed by connecting m unit cells and n unit cells of the 2D graphite which are aligned along $\vec{e}_1$ and $\vec{e}_2$, respectively. So the (m,n) tube defined in Ref. 13 is formed there. The bar j for $1\leqslant j\leqslant l_1$ is defined as that made by adding $(j-1)$ unit cells and one atom along the direction of $\vec{e}_1$ to the bottom of the bar 0. For $j\geqslant l_1+1$, the bar j is made from the bar l_1 by exchanging (l_2-1) unit cells and one atom along $\vec{e}_1$ with l_2 unit cells along $\vec{e}_2$. The network made in this way represents the junction of the (m,n) tube $(j\leqslant 0)$ and the (m_2,n_2) tube $(j\geqslant l_1+1)$, where $l_1=(m_2+n_2)-(m+n)\geqslant 0$ and $l_2=n_2-n\geqslant 0$. This junction is called an (m,n)-(m_2,n_2) junction hereafter. The condition $n_2\geqslant n$ does not lose generality because the (m,n)-(m_2,n_2) junction is the mirror image of the (n,m)- (n_2,m_2) junction. A seven-membered ring is formed at the bottom of the bar 1 and a five-membered ring is introduced between the bar l_1 and the bar l_1+1. There are only six membered rings elsewhere. Based on this bond network, we use a simple tight-binding model including only π orbitals with a common hopping integral and site energy which are used as the unit and the origin of the energy, respectively. In order to get more accurate results, the effects from the mixing with σ orbitals caused by the curvature of the graphitic plane also have to be considered. But these are minor effects compared to those from the *connectivity* of the bond network if the curvature is small. For example, the one-dimensional band structures of a helically coiled nanotube are calculated with the simple tight-binding model including only the π orbitals and with the model including both of the σ and π orbitals in Ref. 3 . The results of the both methods qualitatively coincide with each other near the Fermi level. So we use the simple tight-binding model which is convenient to focus on the effects caused by the topological disorder.

The Schrödinger equation is $Ea_i=-\Sigma_j' a_j$, where a_i is the amplitude at the site i and the sum about j is restricted to the nearest neighbors which are connected with the site i directly by the bonds described above. The number of the nearest neighbors is three for any of the sites. In the present paper, the junctions which are not doped are considered. Then the Fermi level E_F coincides with the common site energies, i.e., zero. The number of atoms in the bar j is $d(j)$ defined as below

$$d(j)=\begin{cases} 2(m+n), & j\leqslant 0 \\ 2(m+n)+2j-1, & 0\leqslant j\leqslant l_1 \\ 2(m+n)+2l_1=2(m_2+n_2), & j\geqslant l_1+1. \end{cases} \quad (1)$$

The amplitudes of the wave function in the bar j are represented by the vector $\vec{c}_j$ whose dimension is $d(j)$. Then Schrödinger equation is written as

$$E\vec{c}_j=P_j\vec{c}_{j-1}+{}^tP_{j+1}\vec{c}_{j+1}+H_j\vec{c}_j, \quad (2)$$

where P_j and H_j are a $d(j)\times d(j-1)$ matrix and a $d(j)\times d(j)$ matrix, respectively. The matrixes P_j and H_j become constant because of the translational symmetry when j is greater than l_1 or less than 1, i.e., $P_j=P_L, H_j=H_L$ $(j\leqslant 0)$ and $P_j=P_R, H_j=H_R$ $(j\geqslant l_1+1)$. The wave function in the tubes of the both ends is described by

$$\vec{c}_j=\sum_{k=1}^{m+n}\{x_{k+}(\lambda_{k+}^L)^j\vec{u}_{k+}^L+x_{k-}(\lambda_{k-}^L)^j\vec{u}_{k-}^L\} \quad (3)$$

for the left tube, $j\leqslant 0$ (Ref. 14) and

$$\vec{c}_j=\sum_{k=1}^{m_2+n_2}\{y_{k+}(\lambda_{k+}^R)^{j-l_1-1}\vec{u}_{k+}^R+y_{k-}(\lambda_{k-}^R)^{j-l_1-1}\vec{u}_{k-}^R\} \quad (4)$$

for the right tube, $j\geqslant l_1+1$, where $\lambda_{k+}=1/\lambda_{k-}$ and $|\lambda_{k+}|\leqslant 1$. The index + (−) means a running wave or a decaying evanescent wave toward the right (the left). In the present paper, we consider conductances at absolute zero temperature of the nanotube junctions which are not doped. Then the tubes in the both ends have to be metallic, i.e., both of $m-n$ and m_2-n_2 have to be multiples of three.[13,15] Otherwise the conductance becomes zero. At the Fermi level, there are extended states only at the K and K' points in the Brillouin zone of the 2D graphite. These states are assigned to $k=1$ and $k=2$ in Eq. (3) and Eq. (4) and all the other states correspond to the evanescent waves. Thus

$$\begin{cases} |\lambda_{k\sigma}^{\mu}|=1, & k=1,2 \\ |\lambda_{k-}^{\mu}|>1, |\lambda_{k+}^{\mu}|<1, & k\geqslant 3. \end{cases} \quad (5)$$

These evanescent waves can be obtained by an analytic continuation of the wave number from the real number space to the complex number space. (See, for example, Eqs. (19)–(22) in Ref. 5). The probability flow from the bar $(j-1)$ into the bar j is written as J_j defined by

$$J_j \equiv \frac{2}{\hbar}\mathrm{Im}({}^t\vec{c}_j{}^* P_j \vec{c}_{j-1}). \tag{6}$$

Conservation of the probability flow at the bar j is represented by

$$\frac{d}{dt}|\vec{c}_j|^2 = J_j - J_{j+1}. \tag{7}$$

In the case of stationary states, the left hand side in Eq. (7) is zero and J_j is constant for arbitrary j, so the flow in the left tube J_j coincides with that in the right tube $J_{j'}$ $(j \leqslant 0, l_1+1 \leqslant j')$. It is represented by

$$\mathrm{Im}\left\{ \sum_{k,k'=1}^{m+n} \sum_{\sigma,\sigma'=\pm} I_{kk'}^{L\sigma\sigma'}(j) x_{k\sigma}^* x_{k'\sigma'} \right\} = \mathrm{Im}\left\{ \sum_{k,k'=1}^{m_2+n_2} \sum_{\sigma,\sigma'=\pm} I_{kk'}^{R\sigma\sigma'}(j') y_{k\sigma}^* y_{k'\sigma'} \right\}, \tag{8}$$

where

$$I_{kk'}^{\mu\sigma\sigma'}(j) \equiv (\lambda_{k\sigma}^{\mu})^* ({}^t\vec{u}_{k\sigma}^{\mu})^* P_\mu \vec{u}_{k'\sigma'}^{\mu} (\lambda_{k\sigma}^{\mu *} \lambda_{k'\sigma'}^{\mu})^j \quad (\mu = R, L). \tag{9}$$

When the following relation holds,

$$I_{kk'}^{\mu\sigma\sigma'}(j) = \{ I_{k'k}^{\mu\sigma'\sigma}(j) \}^*, \tag{10}$$

the imaginary parts of the cross terms in the sum of Eq. (8) cancel out. It can be proved that the relation (10) holds if the condition

$$(\lambda_{k\sigma}^{\mu})^* \lambda_{k'\sigma'}^{\mu} \neq 1 \tag{11}$$

is satisfied. For details of this proof, see Appendix. As can be shown from the relation (5), there are two kinds of terms for which the relation (11) does not hold so that this cancellation may not occur. One is the terms for $\sigma \neq \sigma', k \geqslant 3, k' \geqslant 3$ caused by the evanescent waves, and the other is those for $k=1,2$, $k'=1,2$ caused by the propagating waves. But it is not necessary to consider the former terms, because x_{k+} and y_{k-} for $k \geqslant 3$, by which the former terms are multiplied, have to be zero to avoid solutions divergent at $|j| \to \infty$. In other words, evanescent waves do not contribute to the probability flow. In the latter case of the propagating waves, the condition (11) is the same as the condition

$$(\lambda_{k\sigma}^{\mu}) \neq \lambda_{k'\sigma'}^{\mu}, \tag{12}$$

since $|\lambda| = 1$. In the present case when E_F lies at the K point and the K' point, $\lambda_{1+} = (\lambda_{1-})^* = (\lambda_{2+})^* = \lambda_{2-} = \exp(i2\pi/3)$. Because of this degeneracy of λ, the condition (12) does not hold when $(k,k') = (1,2)$, $(2,1)$, and $\sigma \neq \sigma'$. But when one takes the appropriate linear combinations of the degenerate states, they satisfy Eq. (10). After all, the imaginary parts of the cross terms in Eq. (8) cancel out owing to Eq. (10), except those of terms $k=k'=1,2$ and $\sigma=\sigma'$.

The imaginary parts which do not cancel out are independent of j. Their values are represented by $v_k^{\mu} > 0$ as $\mathrm{Im}\{I_{kk}^{\mu++}\} = -\mathrm{Im}\{I_{kk}^{\mu--}\} \equiv (v_k^{\mu})^2$, where $k=1,2$, $\mu = R, L$. Normalized amplitudes are defined by $\tilde{x}_k = v_k^L x_k$ and $\tilde{y}_k = v_k^R y_k$, so that each extended state has the unit flow. Then Eq. (8) is transformed to

$$\sum_{k=1}^{2} (|\tilde{x}_{k+}|^2 - |\tilde{x}_{k-}|^2) = \sum_{k=1}^{2} (|\tilde{y}_{k+}|^2 - |\tilde{y}_{k-}|^2). \tag{13}$$

The outgoing waves $\tilde{x}_{k-}$, $\tilde{y}_{k+}$ are determined by the incoming waves $\tilde{x}_{k+}$, $\tilde{y}_{k-}$ as

$$\begin{pmatrix} \tilde{x}_- \\ \tilde{y}_+ \end{pmatrix} = \begin{pmatrix} r & t' \\ t & r' \end{pmatrix} \begin{pmatrix} \tilde{x}_+ \\ \tilde{y}_- \end{pmatrix} \equiv S \begin{pmatrix} \tilde{x}_+ \\ \tilde{y}_- \end{pmatrix}, \tag{14}$$

where r, r', t, and t' are 2×2 matrices. Equation (13) guarantees that the 4×4 matrix S is unitary. The conductance σ is obtained from the S matrix by Landauer's formula below:

$$\sigma = \frac{e^2}{\pi\hbar} \sum_{i,j=1}^{2} |t_{ij}|^2 = \frac{e^2}{\pi\hbar} \sum_{i,j=1}^{2} |t'_{ij}|^2. \tag{15}$$

So the range of the conductance is $0 \leqslant \sigma \leqslant 2e^2/(\pi\hbar)$. About conductances shown in this paper, the unitarity of the calculated S matrix, which indicates the accuracy of the numerical calculation, is confirmed to be very good.

The S matrix can be obtained by a recursive calculation of matrix inversion.[16] But details of the method are different from those of Ref. 16. These differences are explained in this paragraph. The wave function in the tubes is represented by

$$\vec{c}_j = \begin{cases} F_L^j \vec{c}_0 & (j \leqslant 0) \\ F_R^{(j-l_1-1)} \vec{c}_{l_1+1} & (j \geqslant l_1+1), \end{cases} \tag{16}$$

where

$$F_\mu = U_\mu \Lambda_\mu U_\mu^{-1}, \tag{17}$$

$$U_{+\mu} = (\vec{u}_{1+}^{\mu}, \vec{u}_{2+}^{\mu}, \cdots), \quad U_{-\mu} = (\vec{u}_{1-}^{\mu}, \vec{u}_{2-}^{\mu}, \cdots),$$

$$U_\mu = (U_{+\mu}, U_{-\mu}), \tag{18}$$

$$\Lambda_\mu = \begin{pmatrix} \lambda_{1+}^{\mu} & & & & & \\ & \lambda_{2+}^{\mu} & & & & \\ & & \ddots & & & \\ & & & \lambda_{1-}^{\mu} & & \\ & & & & \lambda_{2-}^{\mu} & \\ & & & & & \ddots \end{pmatrix} \quad (\mu = L, R). \tag{19}$$

Equations (2) for $j = 0 \sim l_1+1$ are represented by

$$\begin{pmatrix} \widetilde{H}_L & {}^tP_1 & & & \\ P_1 & H_1 & {}^tP_2 & & \\ & \ddots & & & \\ & P_{l_1} & H_{l_1} & {}^tP_{l_1+1} & \\ & & P_{l_1+1} & \widetilde{H}_R & \end{pmatrix} \begin{pmatrix} \vec{c}_0 \\ \vec{c}_1 \\ \vdots \\ \vec{c}_{l_1} \\ \vec{c}_{l_1+1} \end{pmatrix} = 0, \tag{20}$$

where

$$\widetilde{H}_L = H_L + P_L F_L^{-1} = -{}^tP_L F_L \tag{21}$$

and

$$\widetilde{H}_R = H_R + {}^tP_R F_R = -P_R F_R^{-1}. \tag{22}$$

In Eq. (20), $\vec{c}_{-1}$ and $\vec{c}_{l_1+2}$ are eliminated by using Eq. (16). Equation (21) and Eq. (22) are derived from equation $H_\mu + {}^tP_\mu F_\mu + P_\mu F_\mu^{-1} = 0$ $(\mu = L,R)$ which comes from Eq. (2) and Eq. (16). Note that numbers of k in Eq. (3) and Eq. (4) are only $(m+n)$ and (m_2+n_2), respectively,[14] so that $U_{+\mu}$ and $U_{-\mu}$ are not square matrixes. The block tridiagonal matrix in the left hand side of Eq. (20) is singular as shown below. In the tubes ($j \leqslant 0$ or $j \geqslant l_1+1$), half of atoms in the bar j connect only with the right bar $j+1$ and the other atoms connect only with the left bar $j-1$. So half of row vectors in ${}^tP_L$, ${}^tP_1$, P_R, and P_{l_1} are zero vectors, respectively. It means that the block tridiagonal matrix in Eq. (20) has $(m+n)$ and (m_2+n_2) zero vectors in the top $2(m+n)$ row vectors and the bottom $2(m_2+n_2)$ row vectors, respectively. When these zero row vectors are removed, Eq. (20) is represented by

$$\begin{pmatrix} \widetilde{h}_L & {}^tp_1 & & & \\ P_1 & H_1 & {}^tP_2 & & \\ & \ddots & & & \\ & P_{l_1} & H_{l_1} & {}^tP_{l_1+1} & \\ & & p_{l_1+1} & \widetilde{h}_R & \end{pmatrix} \begin{pmatrix} \vec{c}_0 \\ \vec{c}_1 \\ \vdots \\ \vec{c}_{l_1} \\ \vec{c}_{l_1+1} \end{pmatrix} = 0, \tag{23}$$

where $\widetilde{h}_L$ and ${}^tp_1$ have $(m+n)$ rows and $\widetilde{h}_R$ and p_{l_1+1} have (m_2+n_2) rows and all of these rows are nonzero vectors. When $\vec{c}_0$ and $\vec{c}_{l_1+1}$ are developed by using Eq. (3) and Eq. (4), Eq. (23) can be transformed to Eq. (24).

$$\begin{pmatrix} \widetilde{h}_L U_{-L}, & {}^tp_1 & & & \\ P_1 U_{-L}, & H_1 & {}^tP_2 & & \\ & \ddots & & & \\ & P_{l_1} & H_{l_1}, & {}^tP_{l_1 U_{+R} 1} & \\ & & p_{l_1+1}, & \widetilde{h}_R U_{+R} & \end{pmatrix} \begin{pmatrix} \vec{x}_- \\ \vec{c}_1 \\ \vdots \\ \vec{c}_{l_1} \\ \vec{y}_+ \end{pmatrix} = \begin{pmatrix} -\widetilde{h}_L U_{+L} \vec{x}_+ \\ -P_1 U_{+L} \vec{x}_+ \\ 0 \\ -{}^tP_{l_1+1} U_{-R} \vec{y}_- \\ -\widetilde{h}_R U_{-R} \vec{y}_- \end{pmatrix}. \tag{24}$$

Then the block tridiagonal matrix in Eq. (24) becomes a nonsingular $N \times N$ matrix where $N = \Sigma_{j=0}^{l_1+1} d(j) - m - n - m_2 - n_2$. The inverse matrix can be calculated efficiently by using the iterative formula below. When a nonsingular matrix X has block matrixes as

$$X = \begin{pmatrix} H & a \\ b & c \end{pmatrix} \tag{25}$$

and the inverse matrix of H is already known as $g = H^{-1}$, the corresponding block matrixes of the inverse matrix X^{-1} represented by

$$X^{-1} = \begin{pmatrix} G_{00} & G_{01} \\ G_{10} & G_{11} \end{pmatrix} \tag{26}$$

can be obtained by formulas shown below:

$$G_{11} = (c - bga)^{-1}, \quad G_{10} = -G_{11} bg,$$
$$G_{01} = -gaG_{11}, \quad G_{00} = g + gaG_{11} bg. \tag{27}$$

In this way, Eq. (24) can be solved, and one can obtain a matrix $\widetilde{S}$, which determines the relation between the coefficients $\{x\}$ and $\{y\}$ as

$$\begin{pmatrix} \vec{x}_- \\ \vec{y}_+ \end{pmatrix} = \widetilde{S} \begin{pmatrix} \vec{x}_+ \\ \vec{y}_- \end{pmatrix}. \tag{28}$$

As already mentioned in the previous paragraph, the probability flow is determined only by the extended states, $k = 1,2$. So the S matrix in Eq. (14) is obtained by extracting the first, second, $(m+n+1)$th, and $(m+n+2)$th rows and columns from the $\widetilde{S}$ matrix in Eq. (28).

III. RESULTS AND DISCUSSION

To investigate the dependence of the conductance of the junctions on the system size and shape, we calculate conductances of various (m,n)-(m_2,n_2) junctions. They are classified as type I where $m = n + 3i$, $n_2 = m_2 + 3j$ and type II where $m = n + 3i$, $m_2 = n_2 + 3j$. The range of the integers

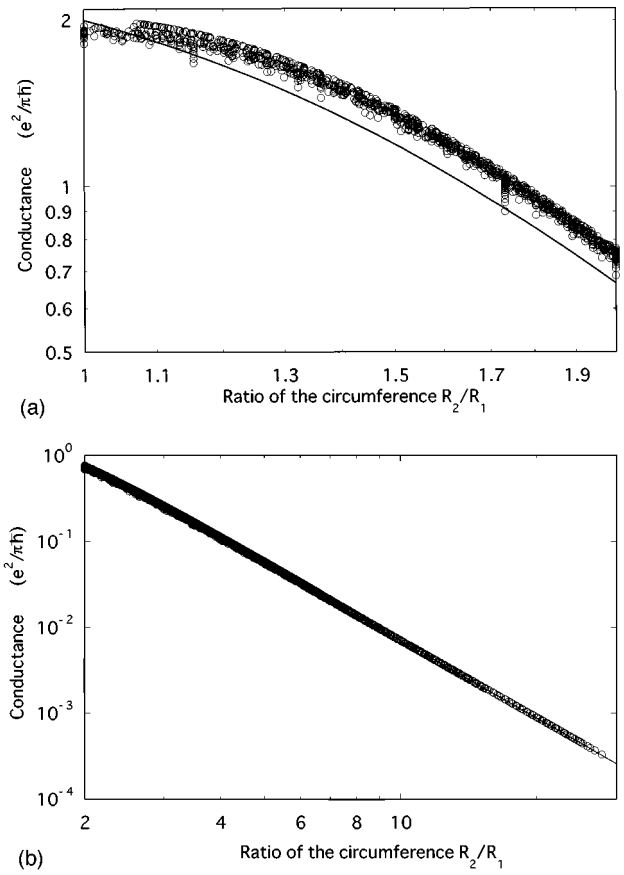

FIG. 2. Conductance as a function of the ratio of the circumferences R_2/R_1 for (a) $R_2/R_1<2$ and (b) $R_2/R_1>2$. Here R_1 and R_2 are the circumference of the thinner tube and that of the thicker tube, respectively. It has been found that the (m,n)-(m_2,n_2) junction has almost the same conductance as that of the (m,n)-(n_2,m_2) junction. Since the two junctions have the same value of R_2/R_1, the conductance of only one of the two is plotted in this figure, so that the number of the plots is reduced and each plot can be distinguished.

i,j,m_2 for the calculations is $i=0$–3, $j=0$–5, $m_2=m_{2\mathrm{in}}-m_{2\mathrm{in}}+20$, where $m_{2\mathrm{in}}$ is the minimum value of m_2 which satisfies the conditions $m_2+n_2\geqslant m+n$ and $n_2\geqslant n$. Here it is not necessary to consider the case when $n>m$ because the (m,n)-(m_2,n_2) junction is the mirror image of the (n,m)-(n_2,m_2) junction, and both of them have the same conductance. The range of the value of the integer n in type I is $n=0$–5, and that in type II is $n=0$–5 when $i\neq j$ and $n=0$–9 when $i=j$. Then the total number of the calculated junctions is about 6000.

Figure 2 shows the calculated conductances of the junctions plotted with the values of R_2/R_1, where $R_1=\sqrt{m^2+n^2+mn}$ and $R_2=\sqrt{m_2^2+n_2^2+m_2n_2}$ are the circumference of the thinner tube and that of the thicker tube, respectively. A clear scaling law is observed in Fig. 2, which will be discussed in more detail latter. The dependence of the calculated conductances on the junction parameters reveals the following features. First, the conductance decreases with the increase of the junction length, when either of the tubes in each side of the junction is fixed. Second, the conductance increases as the circumferences of both the tubes become larger, when the length of the junction is fixed. As the length and the circumference of the junction have opposite effects on the conductance, it is expected that the conductance is kept constant when both the length and the circumference of the junction are made longer or shorter, keeping a certain relation. According to this idea, we have calculated the conductance of about eight hundred kinds of the (m,n)-$(m+i,n+i)$ junctions in the preceding letter,[17] and found a scaling law that the conductance is almost determined by the ratio i/R_1, where R_1 is the circumference of the thinner tube and i represents the length of the junction. But it does not seem natural that the circumference of the thinner tube appears in the scaling law while that of the thicker tube does not, since there is no reason to consider that the thinner tube is more important than the thicker tube. In fact, this scaling law cannot be necessarily applied to more general junctions where $m-m_2\neq n-n_2$. In the present paper, we have found the more complete scaling law as the function of the ratio R_2/R_1. This scaling law does not conflict with the result of Ref. 17, because R_2-R_1 is approximately proportional to the length of junction i.[18] The scaling law of Ref. 17 is a special case of that of the present paper.

As shown in Fig. 2, the conductance σ depends only on the ratio R_2/R_1. This is represented by a dimensionless scaling function f, as

$$\sigma=\frac{e^2}{\pi\hbar}f\left(\frac{R_2}{R_1}\right). \tag{29}$$

The scaling law can be represented by another form using a dimensionless conductance $g(R_2)=f(R_2/R_1)$ with a fixed R_1 as

$$\frac{d\ln g(R_2)}{d\ln R_2}=\beta(g(R_2)), \tag{30}$$

where β has only one parameter g. The initial condition of the scaling equation (30) is

$$g(R_1)=2. \tag{31}$$

It means that when $R_2=R_1$, the length of the junction becomes zero so that g has its maximum value, which corresponds to the complete transmission.[19] If the integral $B(g)=\int^g[dg/g\beta(g)]$ and its inverse function B^{-1} can be obtained, $g(R_2)$ is represented by only one parameter that is the ratio of the circumference R_2/R_1 as

$$g(R_2)=f(R_2/R_1)=B^{-1}\left[\ln\left(\frac{R_2}{R_1}\right)+B(2)\right]. \tag{32}$$

The results of the numerical calculations can be well reproduced by assuming the form of the function $\beta(g)$ as

$$\beta(g)=-\gamma(1-\alpha g). \tag{33}$$

By substituting β of Eq. (33) for Eq. (30), $g(R_2)$ can be obtained analytically as

$$g(R_2)=f(R_2/R_1)=2\left[2\alpha+(1-2\alpha)\left(\frac{R_2}{R_1}\right)^{\gamma}\right]^{-1}. \tag{34}$$

The calculated data in Fig. 2 shows that the function $g(R_2)$ should have the form $7(R_2/R_1)^{-3}$ when $R_2\gg R_1$. Thus we

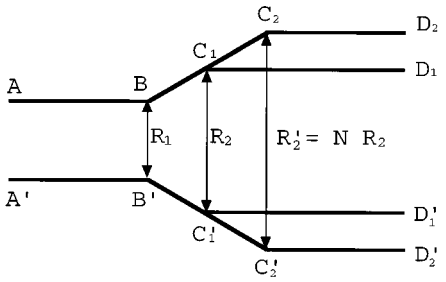

FIG. 3. The scheme of transformation of a nanotube junction. The figure $ABC_1D_1-A'B'C_1'D_1'$ represents a projection map of the junction which is the same as that of Fig. 1 in Ref. 11. To form the junction joining the tubes whose circumferences are $BB'=R_1$ and $C_1C_1'=R_2$, the line ABC_1D_1 is connected with the line $A'B'C_1'D_1'$ so that the points A,B,C_1, and D_1 coincide with the points A',B',C_1', and D_1', respectively. Then a seven-membered ring defect and a five-membered ring defect are introduced at $B(B')$ and $C_1(C_1')$, respectively. When the thinner tube $AB-A'B'$ is fixed and the distance between the five-membered ring defect and seven membered ring defect is made longer, the junction $ABC_1D_1-A'B'C_1'D_1'$ is transformed into a larger junction $ABC_2D_2-A'B'C_2'D_2'$. The original junction $ABC_1D_1-A'B'C_1'D_1'$ is embedded in the transformed junction $ABC_2D_2-A'B'C_2'D_2'$. The circumference of the thicker tube of the transformed junction becomes N times as long as that of the original junction.

take the value of the parameters as $\gamma=3$ and $\alpha=5/14$. This form of $g(R_2)$ are shown in Fig. 2 by the full line. Though the numerical data are fitted well by the analytical curve, the deviation between them becomes slightly larger when $R_2/R_1<2$ than when $R_2/R_1>2$. But the fitting will be improved if higher terms of g are included in Eq. (33).

The origin of the scaling law can be understood intuitively as below. Consider the transformation shown in Fig. 3, where the circumference of the thicker tube C_2C_2' is enlarged N times as large as that of the original one C_1C_1'. This transformation is realized by increasing the distance between the five-membered ring and the seven-membered ring keeping their relative direction and the circumference of the thinner tube fixed. Here and in the following, the junction is represented by a pair of the circumferences of the tubes in the both ends. The original junction (R_1,R_2) is embedded in the transformed junction (R_1,NR_2). Equation (30) is equivalent to the fact that the conductance of the transformed junction $g(NR_2)$ is determined only by N and $g(R_2)$. Though this discussion is similar to that of the scaling theory for the Anderson localization,[20] the functional form of $\beta(g)$ shown in Eq. (33) is quite different from that of the Anderson localization. This difference shows that the scattering process of the electron in the present problem is different from that of the Anderson localization problem.

The scaling law has a remarkable feature that the conductance decays with an increase of R_2 as R_2^{-3} when $R_2 \gg R_1$. Since the length of the junction is approximately proportional to R_2-R_1 as seen in Fig. 3, it means that the conductance decays as the inverse third power of the length of the junction when $R_2 \gg R_1$. This result suggests that the wave function in the junction also shows a power-law decrease as a function of the distance from the contact region with the

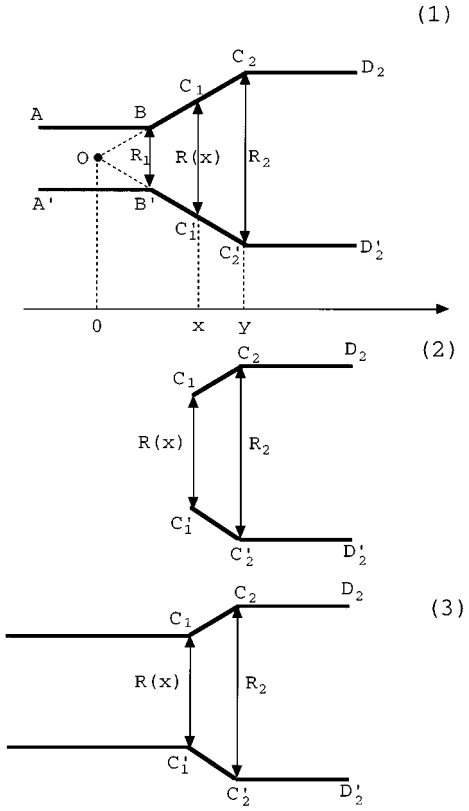

FIG. 4. The scheme showing the relation between the transmission rate and the wave function, when the electronic wave is incident from the thicker tube. Each figure of (1), (2), and (3) are projection maps similar to Fig. 3. See text for detail.

tube. One may consider that the distance mentioned here should be measured from the tube from which the electron is incident. But surprisingly it is not true when the electron is incident from the thicker tube as shown below. The distance related to the power-law decrease of the wave function should always be measured from the thinner tube. To understand this from the scaling properties, consider the junctions (R_1,R_2) and the junction $(R(x),R_2)$ in Fig. 4, on which a unit flow of an electron wave is incident from the thicker tube. The latter junction $(R(x),R_2)$ is formed from the former junction (R_1,R_2) in the following way as seen in Fig. 4. (1) Cut the junction along C_1C_1'. (2) The left half of the junction $ABC_1C_1'B'A'$ is removed. (3) The tube with its circumference $R(x)$ is connected as the new thinner tube at C_1C_1'. Here x means the distance between the cross section C_1C_1' and the point O, and $R(x)$ is the length of the cross section $|\overrightarrow{C_1C_1'}|$. The definition of the point O is as below. When only a five-membered ring is introduced in the thicker tube instead of a pair of a five-membered ring and a seven-membered ring, the circumference of the thinner tube becomes zero and a part of a cone, which is represented by OC_2C_2' in Fig. 4, is formed at the end of the nanotube, instead of a junction. Then the point O is defined as the vertex of the cone.[11]

The norm of the wave function on the cross section C_1C_1' in the original junction (R_1,R_2) becomes the source of the transmitted wave in the newly formed junction

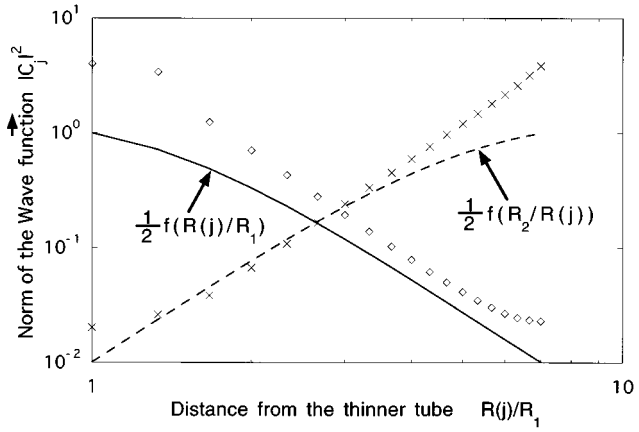

FIG. 5. The norm of the wave function $|c_j|^2$ for the (0,3)-(0,21) junction. For a definition of $\vec{c}_j$ and j, see Fig. 1 and Eq. (2). The diamond plots correspond to the case where the electron is incident from the thinner tube and the cross plots correspond to the case where the electron is incident from the thicker tube, respectively. In each case, there are two kinds of the incident waves corresponding to the K and K' points, which cause two wave functions. But they have common values of $|\vec{c}_j|^2$ because one of them is the mirror image of the other with respect to the mirror plane that the $(0,n)$-$(0,n_2)$ junctions have. The full line and the dotted line show the scaling functions $f(R(j)/R_1)$ and $f(R_2/R(j))$, respectively. The horizontal axis is $R(j)/R_1$, which represents the distance from the point O. For the definition of the point O, see Fig. 4 and text. Here R_1, R_2, and $R(j)$ are the circumference of the thinner tube, that of the thicker tube, and the length of the j'th bar, respectively. That is to say, $R_1=3$, $R_2=21$, and $R(j)=3+j$.

$(R(x),R_2)$. Thus the transmission rate per channel $f(R_2/R(x))/2$ and the norm $|\vec{c}(x)|^2$ are almost proportional to each other, where $\vec{c}(x)$ represents the amplitudes of the wave function at the cross section C_1C_1' and corresponds to $\vec{c}_j$ in Eq. (2). When the incident wave comes from the thinner tube, $f(R(x)/R_1)$ and $|\vec{c}(x)|^2$ are almost proportional to each other, as can be shown from the similar discussion considering the junction $(R_1,R(x))$ as the newly formed one. When $R(x)\gg R_1$ $(R(x)\ll R_2)$, $f(R(x)/R_1)$ $(f(R_2/R(x)))$ is almost proportional to $R^{-3}(x)$ $(R^3(x))$ as can be seen from Eq. (34). Then the norm of the wave function $|\vec{c}(x)|^2$ is almost proportional to $R^{-3}(x)(R^3(x))$ when the electron is incident from the thinner tube (the thicker tube). It means that the norm of wave function decays as x^{-3} (x^3), since $R(x)$ and x is proportional to each other. Note that the distance from the thicker tube, for example, $y-x$ in Fig. 4 (1), does not appear in the power-law decay rule, even when the electron is incident from the thicker tube.

To confirm this discussion, the norm of the wave function in each bar $|c_j|^2$ is plotted as a function of $R(j)/R_1$ in Fig. 5 for the (0,3)-(0,21) junction where $R_2/R_1=7$. For definition of $\vec{c}_j$ and j, see Fig. 1 and Eq. (2). The $R(j)$ represents the length of the bar j, and $R(j)=3+j$, $R(0)=R_1=3$, and $R(19)=R_2=21$ $(j=0,1,\cdots,19)$ in the present case in units of $|\vec{e}_1|$ in Fig. 1. The diamond plots correspond to the case where the electron is incident from the thinner tube and the cross plots correspond to the case where the electron is incident from the thicker tube, respectively. These plots show that the norm of wave function $|\vec{c}_j|^2$. The norm in the former case and that in the latter case are almost proportional to $R(j)^{-3}$ and $R(j)^3$, respectively. For comparison, $f(R(j)/R_1)/2$ and $f(R_2/R(j))/2$ are shown by the real line and the dotted line, respectively. Their behaviors are similar to those of $|\vec{c}_j|^2$, and they show that the above discussion relating the norm of the wave function to the scaling law is reasonable.

All the above discussion is valid when the junction is not doped, i.e., when the Fermi energy E_F is fixed to the common site energy, which corresponds to the K and K' points in 2D Brillouin zone of the graphite. In this case, the number of the channels of any metallic nanotubes is kept at two and independent of the diameter of the tube. When the Fermi energy is shifted by doping, the number of the channels increases as the tube becomes thicker. Our next concern is how the conductance changes when the Fermi energy changes. But it would go beyond the purpose of the present paper to follow up this problem further. Thus we only point out here that it is necessary that the junction is not doped for the one parameter scaling law to hold.

In this work, the conductances of the various nanotube junctions formed by a pair of disclinations, the five-membered ring and the seven-membered ring, are obtained and they are described concisely by the scaling law; they are determined only by a single parameter, i.e., the ratio R_2/R_1, where R_1 is the circumference of the thinner tube and R_2 is that of the thicker tube. When this ratio is large, the conductance is nearly proportional to $(R_2/R_1)^{-3}$. It means that the conductance decays as the inverse third power of the length of the junction when $R_2\gg R_1$. The wave function shows the same power-law decay. The norm of the wave function is almost proportional to x^{-3} and x^3 when the electron is incident from the thinner tube and the thicker tube, respectively, where x is the distance measured from the thinner tube. These results are valid when the Fermi energy lies at the K and K' points of the Brillouin zone, i.e., when the junctions are not doped.

ACKNOWLEDGMENTS

We would like to thank K. Akagi, Dr. S. Ihara, and Dr. S. Itoh for useful suggestions and discussions. This work was supported in part by a Grant-in-Aid from Ministry of Education, Science and Culture, Japan. One of the authors (R.T.) acknowledges the Japan Society for the Promotion of Science for Young Scientists.

APPENDIX: PROOF OF EQ. (9)

The index of $\mu=L,R$ is omitted in the following proof of Eq. (10) for simplicity. For example, P_L or P_R is represented by P. The pair of indexes (k,σ) is concisely represented by k. Since the wave function $c_j=(\lambda_k)^j\vec{u}_k$ satisfies the Schrödinger equation (2) in the tube, the relation

$$(H+\lambda_k^{-1}P+\lambda_k{}^tP)\vec{u}_k=0 \tag{A1}$$

holds, which is equivalent to

$${}^t\vec{u}_k^*\{H+(\lambda_k^*)^{-1}{}^tP+\lambda_k^*P\}=0. \tag{A2}$$

Using this equation, it is shown that

$$I_{kk'}(j)=({}^t\vec{u}_k)^*\{-H-(\lambda_k^*)^{-1}\,{}^tP\}\vec{u}_{k'}(\lambda_k^*\lambda_{k'})^j$$
$$=-{}^t\vec{u}_k^*Hu_{k'}(\lambda_k^*\lambda_{k'})^j-\lambda_{k'}{}^t\vec{u}_{k'}P(\vec{u}_k)^*(\lambda_k^*\lambda_{k'})^{(j-1)}. \quad \text{(A3)}$$

The second term in the last line of the above equation coincides with $-I_{\tilde{k}'\tilde{k}}(j-1)$, where $\vec{u}_{\tilde{k}}=\vec{u}_k^*$ and $\lambda_{\tilde{k}}=\lambda_k^*$. When the first term is represented by $H_{kk'}(j)$, Eq. (A3) becomes

$$I_{kk'}(j)=-H_{kk'}(j)-I_{\tilde{k}'\tilde{k}}(j-1). \quad \text{(A4)}$$

When the second term is transformed again in the same way, one can get

$$(\alpha_{kk'}^2-1)I_{kk'}(j-2)=(1-\alpha_{kk'})H_{kk'}(j-1), \quad \text{(A5)}$$

where $\alpha_{kk'}\equiv\lambda_k^*\lambda_{k'}$ and the relations $I_{kk'}(j)=\alpha_{kk'}^2I_{kk'}(j-2)$, $H_{kk'}(j)=\alpha_{kk'}H_{kk'}(j-1)$, and $H_{\tilde{k}'\tilde{k}}(j-1)=H_{kk'}(j-1)$ are used. If $\alpha_{kk'}\neq 1.0$ then

$$I_{kk'}(j-2)=-H_{kk'}(j-1)/(\alpha_{kk'}+1), \quad \text{(A6)}$$

which shows $I_{k'k}(j-2)=\{I_{kk'}(j-2)\}^*$ because $\alpha_{k'k}=\alpha_{kk'}^*$ and $H_{k'k}(j-1)=\{H_{kk'}(j-1)\}^*$.

[1] S. Iijima, Nature (London) **354**, 56 (1991).

[2] S. Amelinckx, X.B. Zhang, D. Bernaerts, X.F. Zhang, V. Ivanov, and J.B. Nagy, Science **265**, 635 (1994); X.B. Zhang, X.F. Zhang, D. Brenaerts, G. Van Tendeloo, S. Amelincks, J. Van Landuyt, V. Ivanov, J.B. Nagy, Ph. Lambin, and A.A. Lucas, Europhys. Lett. **27**, 141 (1994); S. Ihara, S. Itoh, and J. Kitakami, Phys. Rev. B **48**, 5643 (1993); K. Akagi, R. Tamura, M. Tsukada, S. Itoh, and S. Ihara, *ibid*. B **53**, 2114 (1996).

[3] K. Akagi, R. Tamura, M. Tsukada, S. Itoh, and S. Ihara, Phys. Rev. Lett. **74**, 2307 (1995).

[4] B.I. Dunlap, Phys. Rev. B **49**, 5643 (1994); S. Iijima *et al.*, Nature (London) **356**, 776 (1992).

[5] R. Tamura and M. Tsukada, Phys. Rev. B **52**, 6015 (1995).

[6] H.W. Kroto, J. R. Heath, S.C. O'Brien, R.F. Curl, and R.E. Smalley, Nature (London) **318**, 162 (1985).

[7] D. Vanderbilt and J. Tersoff, Phys. Rev. Lett. **68**, 511 (1992); A.L. Mackay and H. Terrones, Nature (London) **352**, 762 (1991).

[8] S. Itoh and S. Ihara, Phys. Rev. B **48**, 8323 (1993); B.I. Dunlap, *ibid.* **46**, 1933 (1992).

[9] L.S. Kuzmin, P. Delsing, T. Claeson, and K.K. Likharev, Phys. Rev. Lett. **62**, 2539 (1989); A.V. Ustinov, S. Lemke, T. Doderer, R.P. Huebener, L.S. Kuzmin, and Yu. A. Pashkin, J. Appl. Phys. **76**, 376 (1994).

[10] R. Tamura and M. Tsukada, Phys. Rev. B **49**, 7697 (1994).

[11] S. Saito, G. Dresselhaus, and M.S. Dresselhaus, Phys. Rev. B **53**, 2044 (1996).

[12] L. Chico, Vincent H. Crespi, Lorin X. Benedict, Steven G. Louie, and Marvin L. Cohen Phys. Rev. Lett. **76**, 971 (1996); L. Chino, Lorin X. Benedict, Steven G. Louie, and Marvin L. Cohen, Phys. Rev. B **54**, 2600 (1996).

[13] M.S. Dresselhaus, G. Dresselhaus, and R. Saito, Solid State Commun. **84**, 201 (1992).

[14] When $(m,n)=(0,6i)$ and i is an positive integer, the (m,n) tube has flat bands without a dispersion for $E=\pm 1$. In this case, the number of the extended states and the evanescent states are only $m+n-2=n-2$. The values of λ corresponding to the flat bands are 0 and ∞. The corresponding wave functions have nonzero amplitudes only at two neighboring bars in the portion of the (m,n) tube described in Sec. III. Such states that have zero amplitude at infinite sites except for finite sites are sometimes called ''ring states.'' When these ring states are placed so that they do not have any nonzero amplitudes in the portion of the (m,n) tube except at the bar 0, they can compensate for the lack of the base wave functions in Eq. (3).

[15] R. Saito, M. Fujita, G. Dresselhaus, and M.S. Dresselhaus, Phys. Rev. B **46**, 1804 (1992); J.W. Mintmire, B.I. Dunlap, and C.T. White, Phys. Rev. Lett. **68**, 631 (1992); N. Hamada, S. Sawada, and A. Oshiyama, *ibid.* **68**, 1579 (1992).

[16] T. Ando, Phys. Rev. B **44**, 8017 (1991); K. Nikolić and A. MacKinnon, *ibid.* **50**, 11 008 (1994).

[17] R. Tamura and M. Tsukada, Solid State Commun. (to be published).

[18] Ref. 17 treats the case when $m_2=m+i$ and $n_2=n+i$. The scaling parameter in the present paper, $R_2/R_1=(1+3i/R_1\{(i/R_1)+[(m+n)/R_1]\})^{1/2}$ is approximately represented by a single value function of i/R_1 which is the scaling parameter of Ref. 17, since $[(m+n)/R_1]$, the range of which is $1\leqslant[(m+n)/R_1]\leqslant 2/\sqrt{3}$, can be considered to be almost constant. Therefore the scaling rule of the preset paper does not conflict with that of Ref. 17.

[19] It is possible to consider junctions where $R_2=R_1$, for example, (m,n)-(n,m) junctions. Their conductances are not rigorously equal to two in units of $e^2/(\pi\hbar)$, but near values to two. Their conductances approach $2e^2/(\pi\hbar)$ as the circumference $R_2=R_1$ becomes larger. These values of the conductance are shown in Fig. 2(a) at $R_2/R_1=1$.

[20] E. Abrahams, P.W. Anderson, D.C. Licciardello, and T.V. Ramakrishnan, Phys. Rev. Lett. **42**, 673 (1979).